A Fourier Approach for Computationally Efficient Modelling of the Operating Envelope in PMSMs

James Goss[1], Unai SanAndres[1], Ibrahim Afinowi [2], Herminder Matharu [2], Alex Michaelides[2], Mohammad Kimiabeigi[3]
[1]Motor Design Ltd, Ellesmere, Shropshire, UK, james.goss@motor-design.com
[2]Jaguar Land Rover Ltd; Banbury Road, Gaydon, UK, iafinowi@jaguarlandrover.com
[3]Newcastle University; Newcastle Upon Tyne, UK, mohammad.kimiabeigi@ncl.ac.uk

***Abstract*— This paper proposes a novel approach to modelling the torque/speed envelope of PMSMs which considers harmonic components in the voltage waveform. The proposed model is computationally efficient and can produce precise results rapidly, the accuracy of the model and improvement over previous dq based techniques is validated against experimental measurements of a 21-slot 14-pole IPM motor for a hybrid electric vehicle. The technique is then applied to a model of a ferrite based PMSM for a 48V application; it is shown how use of the dq method here can give a significant over estimation of the available peak power when compared to the Fourier approach.**

Keywords— Torque/Speed Curve, Field Weakening, PMSM

I. Introduction

The design of brushless AC PM motors for traction applications requires consideration of performance across the entire operational envelope that commonly includes a field weakening region. Modern design workflows include modelling of peak torque/speed characteristics, efficiency maps, duty cycles and thermally limited torque/speed envelopes. Previous work has shown how a set of techniques, based on the dq model, can be used to rapidly evaluate a candidate motor design over the full operating region [1]–[3]. In these previous approaches the model used to evaluate the maximum torque/amp operating point assumes a sinusoidal flux linkage waveform with no higher order harmonic components and hence a sinusoidal voltage waveform as,

$$v = \frac{d\psi}{dt} = \omega_m \frac{d\psi}{d\theta}. \quad (1)$$

Where v is the instantaneous voltage for one phase, ω_m is the electrical frequency in rad/s, ψ the phase flux linkage and θ the rotor position in electrical degrees.

However in many PM machines, this sinusoidal flux linkage and voltage waveform assumption is not correct. This is particularly true in common slot/pole combinations used in automotive applications such as 2 slots/pole/phase distributed winding machines with a single layer winding or 0.5 slots/pole/phase concentrated winding machines. These machines can exhibit significant harmonics in the voltage waveform which are most prominent during extreme field weakening. These harmonics can be reduced by skewing, typically through the use of offset rotor slices. However, the skewing technique does not completely eliminate the harmonic components in the voltage waveform. These harmonic components can have a significant effect on the operating point of the machine, particularly in the field weakening region, reducing the available peak power.

This paper proposes a set of techniques which allows engineers to rapidly evaluate machine performance across the full operating envelope while accounting for harmonic components in the flux linkage and voltage waveform.

II. Definition of Motor Operating Point

To model a BLAC PM motor across the full operating envelope a control strategy needs to be applied to the model. The maximum torque operating point at any given speed and maximum current magnitude can be described with an optimisation problem characterised by,

maximise

Torque

subject to

$V_{lim} >= V_{phase}$

and

$I_{smax} >= I_{ph}$

Here V_{lim} is the maximum available rms phase voltage available from the inverter, V_{phase} is the rms motor phase voltage, I_{smax} is the maximum phase current and I_{ph} is the motor phase current.

To solve the optimisation problem described above a model of the variation of torque and voltage with current magnitude, I_s, and phase advance angle, γ, is required. Previously this has been achieved using a dq phasor diagram based model:

$$T = \frac{m}{2} p\left(\psi_d I_q - \psi_q I_d\right) \quad (2)$$

$$V_{ph} = \sqrt{V_d^2 + V_q^2} \quad (3)$$

where m is the number of phases and p the number of pole pairs.

Here,

$$V_d = \omega_m \psi_q + R_{ph} I_d \quad (4)$$

$$V_q = \omega_m \psi_d + R_{ph} I_q. \quad (5)$$

Using a curve fitting or interpolation function the variation of ψ_d and ψ_q with I_d and I_q can be mapped and used with (2-3) to compute torque and voltage while accurately modelling saturation and cross saturation effects. However this approach is not able to account for higher order harmonic components.

Fig. 1 shows the 3-phase flux linkage and the transformed dq components for a typical 48 slot 8 pole PM machine at one operating condition across the electrical cycle. It can be seen that, in this case, the flux linkages are not sinusoidal and the harmonic content is present in both the 3-phase and dq waveforms. Previous approaches have averaged the dq components across the full cycle and used with the optimisation problem described above to compute the machine operating point [1], [4].

Fig.2 shows the voltage waveform derived from the flux linkages shown in Fig.1 using (1). As can be seen there are significant harmonics in the voltage waveform with 5th, 7th, 9th, 11th and 13th components present.

Table I shows a comparison between the voltage calculated using the dq flux linkages averaged over the electrical cycle from Fig. 1 with (3) and the rms voltage calculated from the waveforms in Fig. 2. By using the averaged flux linkages with (3) the voltage is underestimated by 8% due to the influence of the harmonics.

Table 1: Comparison between dq and waveform derived voltages

	From ψ_d, ψ_q (Fig. 1)	From RMS of V_a (Fig.2)
Voltage (V_{rms})	126.3	137.0

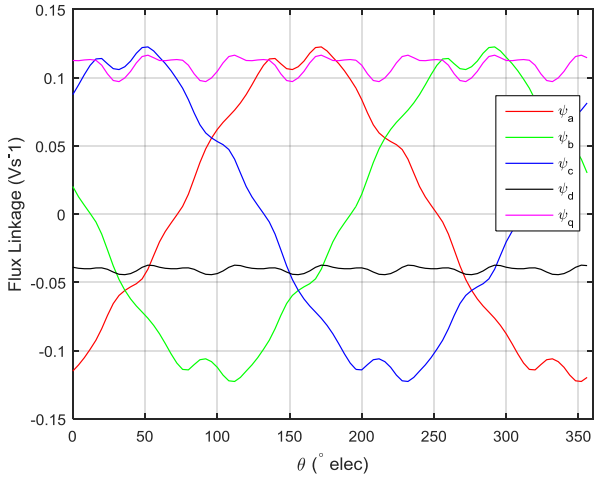

Fig. 1. Three phase flux linkages including dq transformation over the electrical cycle

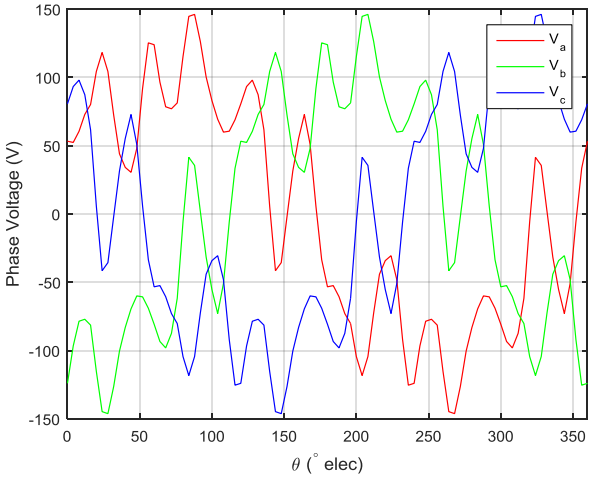

Fig. 2. Voltage waveforms derived from flux linkages over the electrical cycle

III. Fourier Modelling Approach

The proposed Fourier model requires several 2D FE simulations to populate the model. In this paper 30 time-stepping simulations are undertaken at different operating points with 6 distinct values of current magnitude, I_s, and 5 values of current advance angle, γ, to generate a 6x5 grid of the flux linkage components. This gives an accurate result with a low computation time, typically in the range of 5-15 minutes on a desktop PC, dependant on model mesh density, symmetry, number of skew slices and the use of multi-core computation. Here the Motor-CAD EMag 2D FE solver has been used.

A. FEA Model Build

For each value of I_s and γ the flux linkage waveform is calculated across the full electrical cycle of the machine using a time-stepping finite element model. It is assumed that each phase is symmetrical and separated by 360/m degrees, where m is the number of phases. As such, only flux linkage data for a single phase is required. For each phase current and angle the harmonic components of the flux linkage waveforms are extracted, using a Fast Fourier Transform algorithm, up-to a maximum harmonic order, *n*:

$$\psi_{a\,fea} = h_{1\,fea} \sin(\theta + p_{1\,fea}) + h_{2\,fea} \sin(2\theta + p_{2\,fea}) \ldots\ldots h_{n\,fea} \sin(n\theta + p_{n\,fea}). \quad (6)$$

where θ is the rotor position in electrical degrees, h_n is the harmonic amplitude and p_n the harmonic angle.

The harmonic angle components, *p*, are then processed with sine and cosine functions from r=1 to r=n.

$$\alpha_{r\,fea} = \sin(p_{r\,fea}) \quad (7)$$

$$\beta_{r\,fea} = cos(p_{r\,fea}) \quad (8)$$

Where *r* is the harmonic order.

This results in 3D matrices for h_{fea}, α_{fea} and β_{fea} mapped against I_s, γ and harmonic order, *r* (with a matrix size 6x5x*n*).

These matrices are used with a bivariate spline interpolation algorithm to create functions for each component (9-11).

$$h_r = f_1(I_s, \gamma, r) \quad (9)$$

$$\alpha_r = f_2(I_s, \gamma, r) \quad (10)$$

$$\beta_r = f_3(I_s, \gamma, r) \quad (11)$$

IV. Interpolated Model Calculation

Once the model build is complete the phase flux linkage can be evaluated at any given value of I_s, γ and θ using (12) to sum all the harmonic components.

$$\psi_a(\theta) = \sum_{r=1}^{n} h_r \sin(r\theta + \tan^{-1}(\frac{\alpha_r}{\beta_r})) \quad (12)$$

Equation (12) is then applied across the full electrical cycle, to reconstruct the flux linkage waveform from the interpolated FE results at any operating point within the range of the model build. This flux linkage waveform will contain all harmonic components up-to the maximum harmonic order, n. To utilise this approach with the maximum torque per amp strategy and compute the machine operating point, the model needs to calculate the machine torque and phase voltage. The torque can be derived from the i-psi loop method (13), [5].

$$T_{av} = \frac{mp}{2\pi} W' \quad (13)$$

Where W' is the energy converted per phase, (i.e. the area of the ellipse in the flux linkage vs. current loci).

Using (1) and differentiating (12) with respect to θ the voltage can be calculated (14).

$$v_a(\theta) = \omega_m \sum_{r=1}^{n} r.h_r \cos(r\theta + \tan^{-1}(\frac{\alpha_r}{\beta_r})) \quad (14)$$

The voltage waveform can then be reconstructed through application of (14) across the full electrical cycle. The rms phase voltage is then computed (15).

$$V_{rms} = \sqrt{\frac{1}{s}\left(\sum_{y=0}^{s} v_a(2\pi\frac{y}{s})\right)} \quad (15)$$

Where s is the number of rotor steps used to construct the waveform.

V. Experimental Validation

This modelling approach is validated with a 21-slot 14-pole concentrated wound interior permanent magnet motor that is designed for a plug-in hybrid electric vehicle (PHEV). The rotor has 2 skewed segments, however higher order harmonics still exist in the voltage waveform particularly during the field weakening region. The rotor skew segments are modelled using a multi-slice 2D FEA technique [6]. The radial cross section for the machine is shown in Fig. 3.

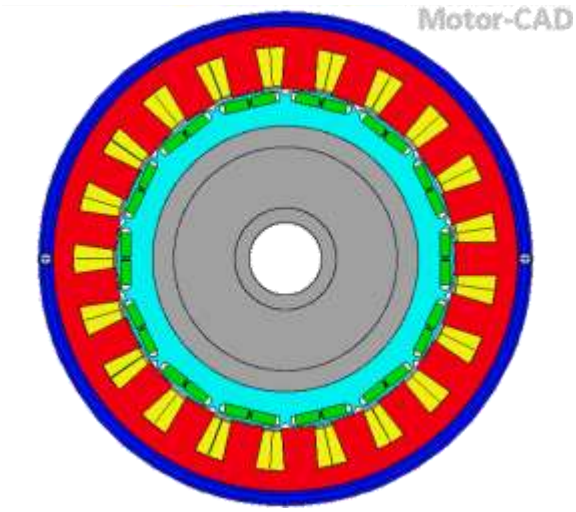

Fig. 3. Radial cross-section for the 21-slot 14-pole PM motor

The torque/speed characteristics of the machine have been tested for given a maximum current with a typical IGBT based inverter at different DC link voltages.

Figs. 4-7 compare the test results to the prediction of the torque/speed and power/speed envelope using both the dq and Fourier methods. In Figs. 4 and 6, while the dq method gives reasonably good estimation of the envelope, at higher speeds and advance angles it consistently over-predicts the torque and power by around 4-5%. Figs. 5 and 7 show how the proposed Fourier method gives an improved estimation of the envelope with very little variation from the test results. In addition it is interesting to note that the shape of the power/speed curve is correctly matched in the Fourier method while the dq method gives a flatter characteristic. This suggests that Fourier method gives a superior representation of the true behaviour of the machine when coupled to an inverter drive.

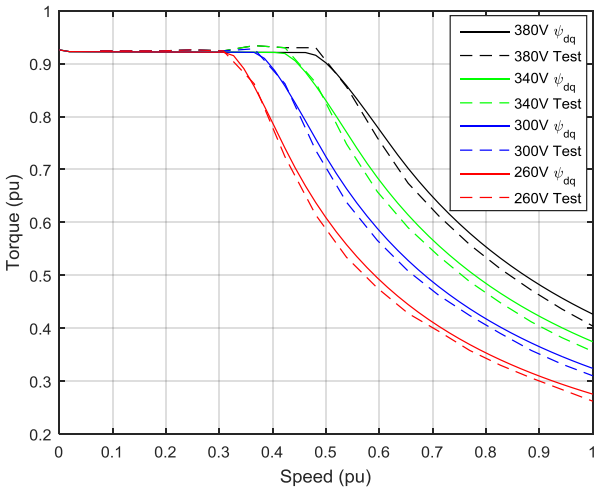

Fig. 4. Comparison of torque/speed characteristics from the dq model and test results

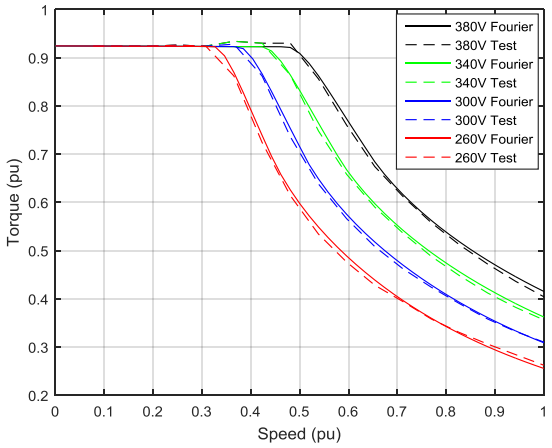

Fig. 5. Comparison of torque/speed characteristics from the Fourier model and test results

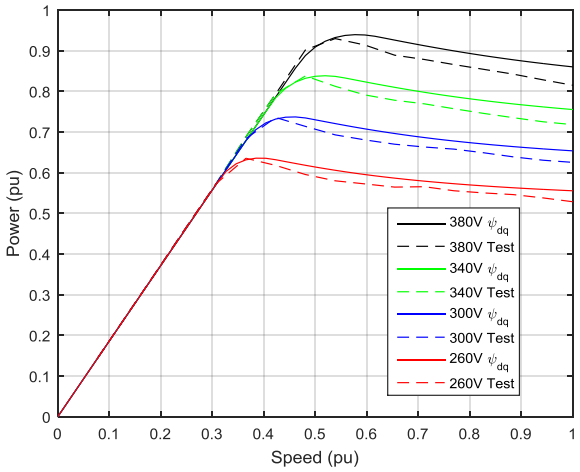

Fig. 6. Comparison of power/speed characteristics from the dq model and test results

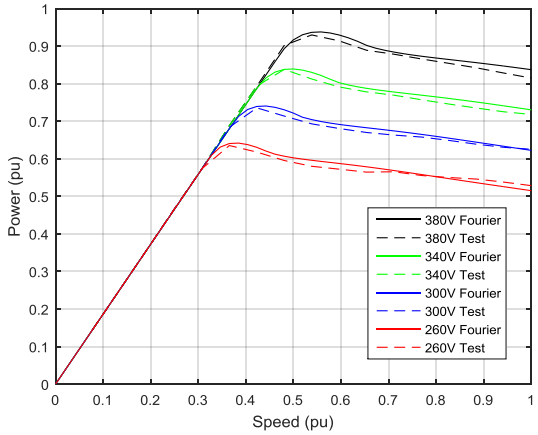

Fig. 7. Comparison of power/speed characteristics from the Fourier model and test results

VI. Comparison of Performance Envelopes for a 48V Machine

A. 48V machine design

48V machines are of interest in automotive mild hybrid (MHEV) applications as they enable a significant reduction in vehicle CO2 emissions at a low cost, particularly if the machine cost can be minimised [7] . However the power required from these 48V systems specifies a very demanding torque/speed curve requirement for the electric machine, often with a constant power speed range ratio (CPSR) >5:1.

Fig. 8 shows the radial cross section of a PMSM for a 48V MHEV P2 application. It has a spoke IPM rotor design and uses ferrite magnets to minimise cost. The spoke type rotor is particularly appropriate for use with low grade magnets which do not have a sufficiently high remanence to saturate the rotor bridges in more typical IPM rotor topologies. However this combination of a spoke rotor and ferrite magnets leads to significant harmonic components in the voltage waveform. These harmonic components coupled with the large CPSR range requirement creates a challenging design problem.

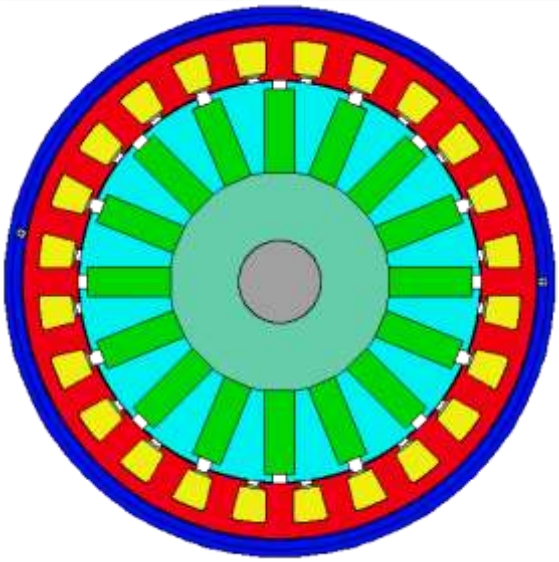

Fig. 8. Radial cross section of the 24-slot 16-pole spoke type PM machine for a 48V MHEV application

B. Performance prediction

The peak torque and power curves for the spoke machine design is shown in Figs. 9 and 10 respectively. They have been predicted using the dq based model approach and the Fourier model. Both models give similar results from 0rpm to the base speed, however when in the field weakening region the prediction is significantly different between the two models. The dq model shows the torque and power continuing from base speed to maximum speed with a relatively flat power characteristic whereas the Fourier model shows that the peak power is achieved soon after the base speed and falls rapidly. The Fourier model predicts that the machine cannot operate

from half speed to maximum speed without violating the voltage limit.

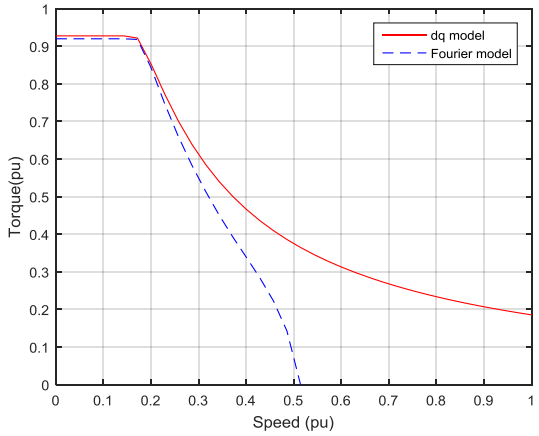

Fig. 9. Predicted torque/speed characteristics with dq and Fourier modelling methods

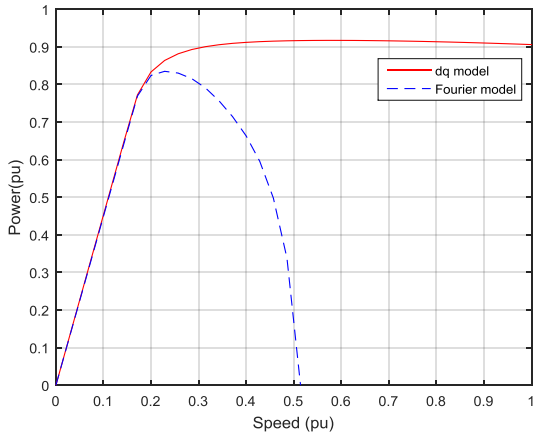

Fig. 10. Predicted power/speed characteristics with dq and Fourier modelling methods

C. Model Validation

To validate the model predictions each point on the torque/speed curve has been compared to a time-stepping FEA calculation, for each point the speed, current magnitude and angle are input into the FEA model and the rms voltage is calculated from the voltage waveform computed over the full electrical cycle.

Fig. 11 shows a comparison between the voltage predicted using the dq model and the voltage from the FEA. At maximum speed the FEA computed voltage is nearly double the voltage predicted from the dq model. Hence, it is clear that the dq model is giving misleading results and that the high speed torque and power predictions cannot be achieved within the given voltage constraints. Fig. 13 shows the harmonic composition of the voltage waveform, calculated from FEA, for the maximum speed operating point predicted by the dq model. The fundamental component is close to the $48V_{pk}$ limit however there is a significant 5^{th} harmonic at 85V and 7^{th} harmonic at 43V. These harmonic components are not supressed by the field weakening mechanism and hence result in a violation of the voltage limit at high speed.

Fig. 12 shows a comparison between the voltage predicted by the Fourier model and the FEA calculation, using the operating points predicted from the Fourier model. There is good correlation between these with the Fourier model accurately accounting for the influence of the harmonic components on the voltage.

These results suggest that this spoke type machine is not capable of operating across the required speed range when driven with a typical sinusoidal inverter drive.

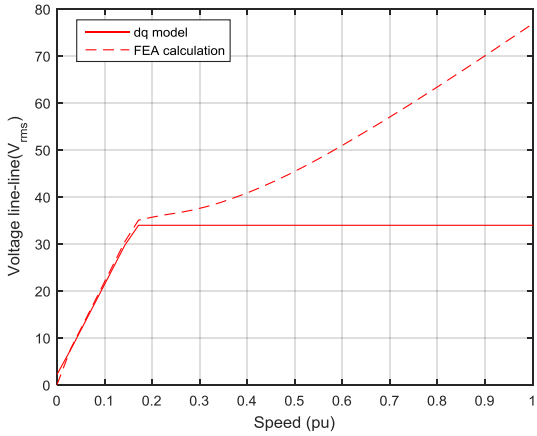

Fig. 11. Comparison between the voltage predicted using the dq model and the voltage from the FEA

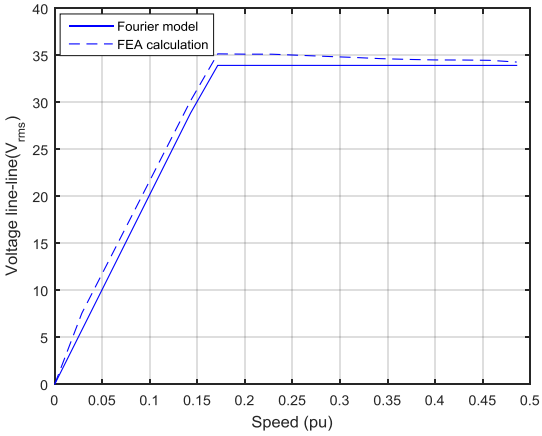

Fig. 12. Comparison between the voltage predicted using the Fourier model and the voltage from the FEA

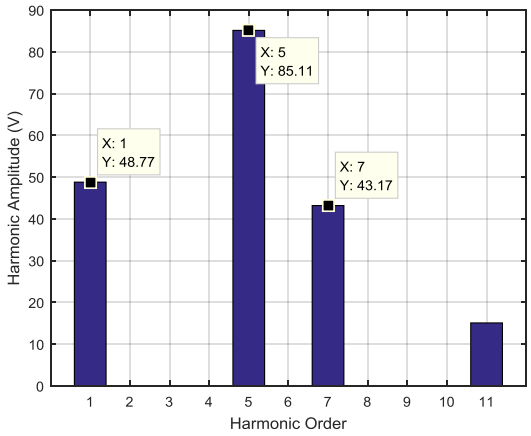

Fig. 13. Harmonic composition of the FEA computed voltage waveform at the maximum speed point predicted by the dq model

VII. Conclusions

This paper has proposed a new method for modelling PMSMs that allows the influence of higher order harmonic components to be accounted for when computing torque/speed characteristics, efficiency maps and duty cycles.

It is shown that in many cases these higher order components can add a significant increase in the rms voltage of the machine and that this leads to a reduction in the machine output power and torque in the field weakening region. The proposed Fourier method is shown to be able to accurately estimate this additional voltage and give a realistic evaluation of the available torque and power of the machine in the field weakening region. The validation exercise with the test results from the 21s14p machine demonstrates that this approach accurately represents behaviour when driven with a typical inverter drive and the validation exercise with the 48V spoke type machine demonstrates that this method correlates well with a time-stepping current driven FEA simulation at each operating point.

The proposed method is computationally efficient and can be used in place of the dq method without a significant increase in computational time. Future work will investigate further into inverter behaviour and non-sinusoidal current waveforms.

References

[1] J. Goss, P. H. Mellor, R. Wrobel, D. A. Staton, and M. Popescu, "The design of AC permanent magnet motors for electric vehicles: a computationally efficient model of the operational envelope," in *6th IET International Conference on Power Electronics, Machines and Drives (PEMD 2012)*, 2012, pp. B21–B21.

[2] E. Dlala, M. Solveson, S. Stanton, Z. Tang, M. Christini, R. Ong, and B. Peaslee, "Efficiency map simulations for an interior PM motor with experimental comparison and investigation of magnet size reduction," in *2013 International Electric Machines & Drives Conference*, 2013, pp. 23–29.

[3] A. Mahmoudi, W. L. Soong, G. Pellegrino, and E. Armando, "Efficiency maps of electrical machines," in *2015 IEEE Energy Conversion Congress and Exposition (ECCE)*, 2015, pp. 2791–2799.

[4] J. Goss, M. Popescu, D. Staton, P. H. Mellor, R. Wrobel, and J. Yon, "A Comparison between Maximum Torque/Ampere and Maximum Efficiency Control Strategies in IPM Synchronous Machines," in *IEEE Energy Conversion Congress and Exposition (ECCE)*, 2014.

[5] D. A. Staton, W. L. Soong, and T. J. E. Miller, "Unified theory of torque production in switched reluctance and synchronous reluctance motors," *IEEE Trans. Ind. Appl.*, vol. 31, no. 2, pp. 329–337, 1995.

[6] S. Williamson, T. J. Flack, and A. F. Volschenk, "Representation of skew in time-stepped two-dimensional finite-element models of electrical machines," *IEEE Trans. Ind. Appl.*, vol. 31, no. 5, pp. 1009–1015, 1995.

[7] R. Wrobel and P. H. Mellor, "Design considerations of a direct drive brushless PM machine with concentrated windings," in *IEEE International Conference on Electric Machines and Drives, 2005.*, 2005, pp. 655–658.